Theoretical Study of $Cu^{I}Y$ Zeolite: Structure and Electronic Properties

Nicolas Jardillier,* Dorothée Berthomieu, and Annick Goursot

Laboratoire de Matériaux Catalytiques et Catalyse en Chimie Organique, UMR 5618, UMI ENSCM-CNRS, 8 rue de l'Ecole Normale, 34296 Montpellier Cedex 5, France

J. Ulises Reveles and Andreas M. Köster

Departamento de Química, Centro de Investigación y de Estudios Avanzados, Av. IPN 2508, Colonia San Pedro Zacatenco 07360, México City D.F., México

Received: June 8, 2006; In Final Form: July 25, 2006

The structural and electronic properties of the accessible Cu^{I} site of a faujasite-type zeolite have been studied, by use of large cluster models and a density functional theory-based methodology. We demonstrate that the local ideal C_3 symmetry of the Cu^{I} site II is broken. The Cu^{I} cation is bonded to the zeolite framework by one bond of about 2.26 Å and two shorter ones of 2.07 Å. We demonstrate that only one cation position exists at this site. This result is also confirmed by a molecular electrostatic potential analysis. We show that local properties at site II, as well as the global properties of the solid (frontier orbitals), do not depend on the Al and cation distribution and only slightly on the cocation nature. Taking into account the present results and well-known experimental data, we propose that specific catalytic behaviors are correlated with local response properties, such as the local acid strength or, in other reactions, specific local architecture or confinement.

I. Introduction

Zeolites are crystalline microporous solids formed from amorphous species in aqueous solution, often called synthesis gel, which contains inorganic silicate and aluminate precursors as well as various cations and anions. The growth of the solid, that is, its crystallization in aqueous medium, proceeds through the continuous dissolution of the gel. The architecture of the synthesized framework depends thus on many parameters, such as time, temperature, pH, and relative amounts of all the ionic species, including the templating agents.[1] Therefore, minimization of dehydrated zeolite models, which provide the most thermodynamically stable structures, does not guarantee one to obtain the "real" solid in terms of Al, Si, and cation distributions. On the other hand, the structure topology is not measurable with X-ray or neutron diffraction techniques, because these experiments yield information only about the average structure of the solid. Substitution of Si by Al (or any other element) in the zeolite framework and the presence of counterions induce only local perturbations to an overall solid symmetry, which remains predominant in the structure determination. Although the replacement of Si by heterotaoms involves modifications of distances and angles around the substituted site, the accurate values of these structural parameters are not accessible experimentally. These structural changes together with their related electronic effects manifest themselves in changes of the ^{29}Si NMR spectra for zeolites with different Si/Al ratios.[2]

Only "ideal" zeolite frameworks that have purely siliceous frameworks or those that have a Si/Al ratio of 1 can be determined experimentally. The former ones have no catalytic or adsorption interest; the latter are highly difficult to synthesize and are limited to few prototypes.[3] Therefore, the development of adequate methodologies for the modeling of the interplay between structures and properties of the solids discussed here still represents a challenge for computational chemistry.

The past decade has seen substantial progress in methodological developments and numerical techniques. Larger systems can be studied with much less computational effort than previously. Structures and, in some cases, properties of several zeolites or aluminophosphates with small or medium-size unit cells (from chabazite, 36 atoms, to ferrierite, 108 atoms) have been studied by use of periodic calculations.[4−10] Larger unit-cell zeolites like mordenite (144 atoms) and ZSM-5 (288 atoms) have also been studied, either fully siliceous[11,12] or with one (Al, cation) site and a guest molecule.[13−17] Mordenite with the natural composition, that is, 8 (Al, Na) per unit cell (152 atoms), has also been investigated.[11] Sn-BEA, with one Sn per unit cell, has also been studied recently.[18] Zeolites such as H-BEA, H-ZSM-5, and H-FAU, containing one (Al, H) site, that is, 193, 289, and 572 atoms, respectively, per unit cell, have been studied recently by use of large clusters[19] or embedded clusters.[20]

Among the zeolites, which are the most involved in industrial catalytic processes, ZSM-5 is a highly siliceous catalyst, with current Si/Al ratios of 20−100; mordenite is used with Si/Al ratios of 8−10, whereas faujasite zeolites of Y type are used with Si/Al ratios of 2.5−3 for deNO_x reactions and 5−6 for acidic catalysis. These values imply that whereas the number of (Al, cation) pairs per unit cell is restricted to 3−14 for ZSM-5, it increases to 13−16 for mordenite and reaches 82−163 for the Y zeolite.

Modeling "real" solids is thus hardly possible, because of the large number of framework plus extraframework ions per unit cell and, more critically, because of all the possible distributions of Al among the framework.

In fact the "real" solid should be considered as a statistical average (taking into account the Löwenstein rule[21]) of all possible models based on different distributions of the (Al, cation) couples in the solid. This is, of course, out of reach presently, either through a periodic or even a large-cluster approach. The results that we are presenting in this paper are

10.1021/jp063568o CCC: $33.50
Published on Web 08/24/2006

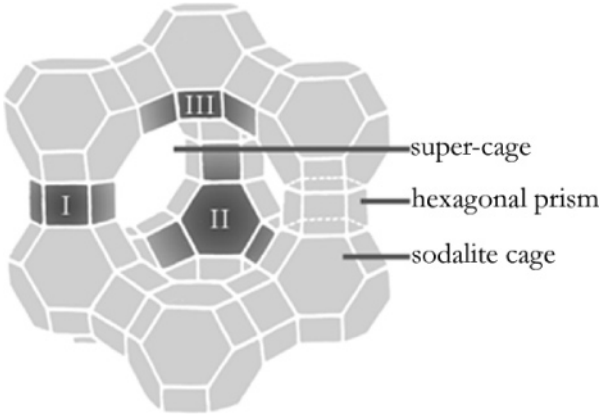

Figure 1. Faujasite-type structure.

connected with this concept but with a restricted focus on the local geometry of an accessible Cu^{I} site of a CuY zeolite, used in oxidoreductive deNO$_x$ catalysis, that is, with a Si/Al ratio of 2.5. A large cluster has been used for this study. The dependence of the Cu^{I} site geometry upon the local Al topology and the nature of the other counterions (H^+ and Na^+) is analyzed in detail through the comparison of structural parameters, molecular electrostatic potential (MEP) values, and electronic properties.

II. Methodology and Models

II.1. Models. The faujasite-type zeolite (FAU) has a three-dimensional framework built from prisms and sodalite cages connected through six-member rings. Figure 1 illustrates these building blocks, which enclose a large pore, with a diameter of about 13 Å, generally called a supercage. Whereas each SiO_4 tetrahedron has a neutral total charge, each AlO_4 introduces a negative charge into the framework, compensated by a counterion that may be either a proton, an organic cation, an alkali, or a transition-metal cation. Two distinct FAU families exist, X zeolites with a Si/Al ratio of approximately 1 and Y zeolites with a Si/Al ratio in the range 2.5−6.0, the most commonly used experimentally. Extraframework cations (not protons) in a Y zeolite are mainly distributed in sites I, II, and III (cf. Figure 1). Each site is classified into subsites.[22−26] The population of these sites depend on several factors such as Si/Al ratio, cation nature, temperature, and possible extraframework molecules (H_2O, NH_3, etc.). Site I, located in the prisms, is almost not accessible to guest molecules,[27,28] in contrast to sites II and III. In Y zeolites, sites III are most probably not or only very little occupied.[25,26] The accessible cations, involved in reactions, are thus located at sites II. As shown in Figure 1, site II is at the center of a six-membered ring that connects the sodalite cage with the supercage. According to the Löwenstein rule,[21] Al−O−Al linkages are forbidden, indicating that the six-membered ring (6T) can contain a maximum of three Al atoms with the distribution 1-3-5. The oxygen and the T (Si or Al) atoms of the 6T ring are labeled from 1 to 6 as shown in Figure 2. Obviously, the distribution can be 1-3, 1-4, or 1-5 (equivalent to 1-3) in the case of two Al atoms in the 6T ring, and 1 in the case of one Al atom.

To study the effects induced by different local distributions in the 6T ring, and thus possible deformations from the C_3 symmetry of the fully siliceous zeolite, large clusters have been employed. They were extracted from a FAU system, with a Si/Al ratio of 2.5, optimized by molecular mechanics using the periodic boundary conditions and a random distribution of Al (Cerius2,[29] cvff_aug_ionic force field). The total number of atoms and cluster compositions are summarized in Table 1. The

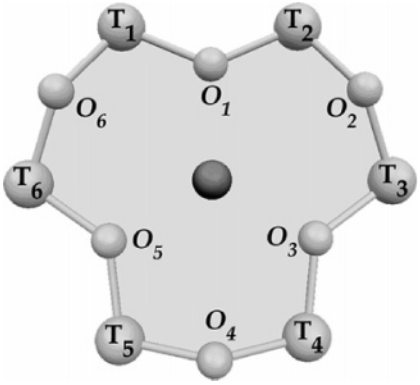

Figure 2. Nomenclature used to describe site II of the FAU-type zeolite.

TABLE 1: Number of Si, Al, O, H, Na, and Cu Atoms for Clusters A−H[a]

	Si	Al	O	H	Na	Cu	distrib
A	31	11	84	9	1	1	1
B	30	12	84	9	2	1	1
C	30	12	84	9	2	1	1-3
D	30	12	84	9	2	1	1-4
E	30	12	84	9	2	1	1-3-5
F	31	11	84	0	10	1	1
G	30	12	84	0	11	1	1
H	30	12	84	0	11	1	1-3

[a] For each cluster (A−H), the local distribution pattern of Al atoms in the 6T ring is given. H atoms are given without H used to terminate clusters.

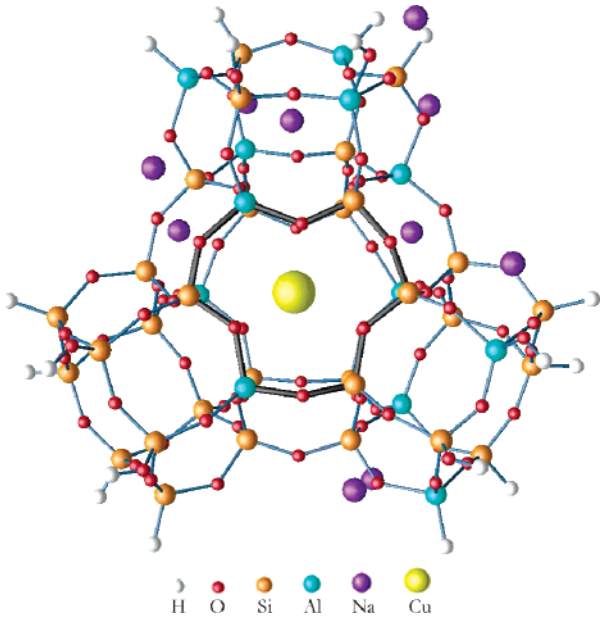

Figure 3. Optimized model clusters for Cu^{I} at site II, model H, with Cu^{I} and Na^+ as counterions. The 6T ring is illustrated by thicker black bonds.

local distribution pattern of the 6T ring is given in this table, too. The dangling bonds of the oxygen, silicon, and aluminum atoms are terminated with H atoms positioned along the O−Si/Al and Si/Al−O bonds at the distance of 1.0 and 1.5 Å, respectively. Clusters labeled from A to H include one sodalite cage and three hexagonal prisms. Figure 3 illustrates cluster H (see Table 1).

II.2. Computational Details. The calculations have been performed with the density functional theory (DFT) program deMon.[30] Geometries have been optimized in redundant coor-

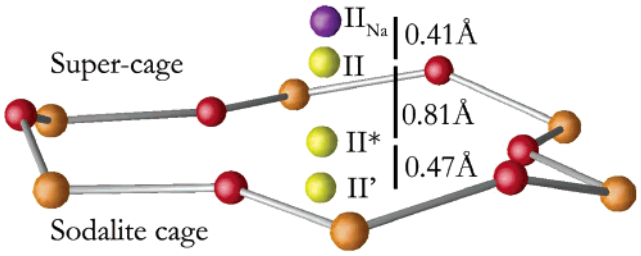

Figure 4. Different cationic positions defined by experiments for site II. Sites II and II* were refined by ref 25; sites II′ and II$_{Na}$, by ref 26.

dinates[31] within the generalized gradient approximation (GGA) of Perdew−Burke−Ernzerhof (PBE)[32] for the exchange and correlation potentials and energies. DZVP-quality basis sets[33] were used for all atoms, and A2 auxiliary functions[33] were used to fit the density. The geometry convergence criteria were 0.001 au for the root-mean-square of the gradient, a maximum gradient of 0.0015 au, and either an energy change smaller than 10^{-7} or a root-mean-square smaller than 0.004 au for the internal displacement associated with a maximum displacement of 0.006 au. The hydrogen atoms terminating the cluster have been kept fixed during the geometry optimization.

III. Results and Discussion

III.1. Experimental Structural Data Available. Experimental data on the crystal structure of Cu^{I}Y reported in the literature are limited. Palomino et al.[25] published the X-ray powder diffraction analysis (XRD) of a dehydrated Cu^{I}Y prepared by reacting NH_4Y with gaseous CuCl at 673 K.[34] These authors defined three crystallographic sites for the Cu^{I} metal cations named I*, II*, and II. Sites II* and II were defined as "just inside the sodalite cage" and "inside the supercage", respectively. Fowkes et al.[26] published a high-resolution powder neutron diffraction (HRND) on a partially exchanged (Cu^{I}/Na)Y zeolite. They identified three sites for Cu^{I} named IA′, IB′, and II′. Site II′ is similar to the position II* defined previously[25] but slightly more inside the sodalite cage. This site II′ and those previously named II* and II by Palomino et al. are illustrated in Figure 4. The position of Na^+ cations found by HRND[26] at site II is also shown (II$_{Na}$) in Figure 4, to illustrate the difference with Cu^{I}. The Rietveld refinements of refs 25 and 26 have been performed by use of the space group $Fd\bar{3}m$. The models obtained thus have a local C_3 axis at site II, on which the Cu^+ or Na^+ cations are located. These cations thus coordinate to three equivalent framework O atoms with identical bond distances. Moreover, the geometric parameters reported for the framework are identical, whether the cations are at site II or site II*,[25] or at sites II′ or II$_{Na}$,[26] which would indicate that two solids with identical frameworks but different framework−cation interaction energies could have similar thermodynamical stabilities.

III.2. Geometry of the Cu^{I} Site. Matching the Si, Al, and O atoms of the 6T ring belonging to our clusters with those of the spectroscopically defined models (by least-squares adjustment) shows that the geometric parameters of the optimized clusters differ from those of the experimental models[25,26] by a maximum of 0.2 Å for oxygen and 0.1 Å for T-atom positions. This discrepancy is the consequence of the indiscernability of Si and Al atoms in XRD and HRND analyses. Indeed, Al−O−Si and Si−O−Si angles differ by approximately 5−10°, and Al−O and Si−O distances differ by about 0.1 Å. This superposition shows also that the Cu^{I} positions in the optimized clusters differ from the XRD model by about 0.15 Å for site II* and 0.95 Å for site II, and from the HRND model by about 0.37 Å for site II′. The data presented in Table 2 show that the local geometry at site II processes no symmetry. The bond distances between Cu^{I} and the three oxygen atoms (O_1, O_3, and O_5) of the framework are not equivalent and vary according to the distribution pattern of the Al atoms in the 6T ring. In fact averaging these three Cu−O bond distances, to "symmetrize" the site, leads to very similar values, 2.12−2.15 Å, for all Al distributions (Table 2). More interestingly, the same value of 2.12 Å is obtained by averaging the experimental Cu−O bond distances of sites II* and II.[25] We can also read the XRD result, that is, three 2.03 Å bonds at site II* and three 2.21 Å bonds at site II, with a double occupancy (0.39/0.18) for site II*, as the result of averaging sites that contain, each, two 2.03 Å and one 2.21 Å bonds. With this interpretation, which does not impose the C_3 symmetry, we can easily compare our results with the experimental data: the average over all models of the two shorter bonds, 2.07 Å, correlates well with 2.03 Å, whereas the averaged longer bond, 2.26 Å, is also very close to the experimental value of 2.21 Å. This analysis shows that when the local Al distribution is taken into account, our approach brings more detailed information while reproducing the experimental XRD data. By comparison with the HRND[26] results, that is, one unique site II′ with three Cu−O bonds of 2.22 Å, we can conclude that the "symmetrized" values, although shorter by about 0.10 Å, remain nevertheless compatible, due to the very large uncertainty of these measurements (see section III.4).

III.3. Clusters A−E. Clusters A−E have all been superimposed in order to evidence differences between their copper positions and, eventually, different possible sites. The maximum distance between their Cu positions is 0.3 Å, for clusters B and

TABLE 2: Bond Lengths, Dihedral Angles,and Averages for Optimized Clusters Cu^{I}Y A−H[a] and Experimental Results

	calcd clusters								exptl results		
	A	B	C	D	E	F	G	H	II* [b]	II[b]	II[c]
no. of Al in 6T	1	1	2	2	3	1	1	2			
distribution	1	1	1-3	1-4	1-3-5	1	1	1-3			
d(Cu−O_1), Å	2.30	2.37	2.09	2.08	2.11	2.19	2.22	2.03	2.03	2.21	2.22
d(Cu−O_3) , Å	2.11	2.09	2.23	2.02	2.20	2.17	2.16	2.33	2.03	2.21	2.22
d(Cu−O_5) , Å	2.02	2.00	2.04	2.26	2.16	2.04	2.02	2.03	2.03	2.21	2.22
∼[d(Cu−$O_{1,3,5}$)] , Å	2.14	2.15	2.12	2.12	2.15	2.13	2.13	2.13	2.12[d]	2.12[d]	2.22
∼[d(Cu−$O_{2,4,6}$)] , Å	2.99	3.00	3.06	3.10	3.11	3.04	3.05	3.05	3.02	3.05	3.03
∠O_1−O_3−O_5−Cu, deg	−0.6	−0.6	0.4	1.5	−1.2	−1.3	−1.8	−1.3	−3.9	−40.9	18.8
∠O_2−O_4−O_6−Cu, deg	19.6	18.7	19.2	17.3	16.0	12.3	8.4	8.9	9.1	20.7	28.3
∼[d(Si−O)] , Å	1.64	1.65	1.65	1.65	1.65	1.64	1.65	1.64	1.665	1.665	1.635
∼[d(Al−O)] , Å	1.77	1.77	1.77	1.78	1.77	1.756	1.76	1.76	1.665	1.665	1.635
∼[∠Si−O−Si], deg	139.1	138.4	138.6	138.7	138.9	139.5	140.0	139.1	137.2	137.2	140.8
∼[∠Al−O−Si], deg	135.5	135.6	135.4	136.2	135.9	134.9	134.6	134.2	137.2	137.2	140.8

[a] With respect to the distribution pattern of Al in the 6T ring. [b] Reference 25. [c] Reference 26. [d] Average value over II* and II Cu−O bond distances.

D, whereas the average variation over all clusters is about 0.18 Å. These values are far from the experimental distance between site II and II* from ref 26, which is 0.81 Å and collinear with the C_3 axis, that is, perpendicular to the $O_1O_3O_5$ plane, whereas the small fluctuations of Cu positions in clusters A−E occur in this plane, as shown in Table 2 ($O_1O_3O_5Cu$ dihedral angle between −1.8° and 1.5°). These small variations reveal changes in the 6T Al distribution. This observation enables us to propose that the clusters describe the effect of different local Al distributions around site II*. Their average could be compared to the idealized C_3 symmetry assumed by all diffraction models. To explore other possible stable Cu positions, Cu has been displaced perpendicularly to the $O_1O_3O_5$ plane, both toward the supercage (by 0.9 Å) and toward the center of the sodalite cage (by 0.6 Å). This procedure was applied to clusters C and D. The displacement amplitude (1.5 Å) includes all positions suggested by experiment. These clusters have then been reoptimized by the same computational procedure as described in section II.2. In all cases, the Cu^{I} cation moves back to its original location.

III.4. Clusters F−H. In clusters F−H, the nine protons have been exchanged with sodium cations. Protons have an impact on the Si−O and Al−O bond lengths, increasing them by about 0.1 Å. It is important to note that, for Y zeolites, experimental cell parameters do not show a strong dependence on the cation nature.[22,24−26]

There is no substantial change in the average Si−O and Al−O bond values between the models A−E and F−H (Table 2), because only 9 out of 108 bonds are influenced by the proton exchanges. Locally, changes in Si−O and Al−O bonds are around 0.1 Å. Nevertheless, the coordination of the Cu ion does not change with the nature of the counterions: very similar Cu positions are obtained for the A−E and F−H clusters, that is, similar site II* positions. This result shows that the nature of the other exchanged cations has little impact on the coordination of the Cu^{I} cation at site II. More generally, we find that the local geometry around Cu^{I} depends slightly on the Al distribution pattern in the 6T ring but not on the nature of the other counterions. To compare our results with the experimental data, we have chosen to represent the experimental uncertainty by use of the isotropic temperature factor, which defines the radius of a sphere centered at the equilibrium position of each atom. The sum of the diameter of these spheres centered at Cu and O (O_1, O_3, O_5) gives a measure of the maximum uncertainty on the Cu−O distance, which is illustrated by the thickness of the bands presented in Figure 5 (light gray, dark gray, and dashed). For every cluster calculated, Cu bonds with O_1, O_3, and O_5 are illustrated with black dots and attributed an uncertainty of 0.06 Å.[35] As mentioned previously, Cu is coordinated to the 6T ring oxygens with one bond of about 2.26 Å and two shorter bonds of 2.07 Å (average value); this average is represented by white dots in Figure 5. This figure highlights that the shortest bonds are mostly included within the experimental uncertainty range of site II* and the longest one within the experimental uncertainty range of site II and II′. For cluster E, all bond lengths are almost equivalent due to a 1-3-5 Al distribution in the 6T ring. For a Si/Al ratio of 2.5 (137 Si/55 Al), this distribution is statistically much less probable than 1-3 and 1-4 and should thus have little representation in the experimental results.

III.5. Electronic Structure Results. The Cu−O bond order values range from 0.20 to 0.33, following the same trend as the Cu−O bond lengths (Tables 2 and 3), that is, three bonds with one slightly weaker.

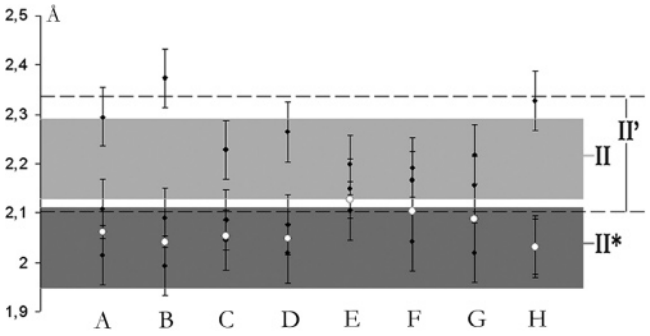

Figure 5. Detailed representation of Cu−O bonds for the clusters A−H: black dots on the vertical bars indicate the calculated $Cu^{I}-O_1$, $Cu^{I}-O_3$, and $Cu^{I}-O_5$ distances, whereas the bar lengths represent the associated uncertainty of 0.06 Å. White dots indicate the average value of the two shortest bond lengths. The dark gray band illustrates the experimental uncertainty for the Cu−O distances of site II*, whereas the light gray band illustrates that of site II (ref 25); the dashed lines mark the uncertainty range for site II′ (ref 26).

For all clusters, the five higher occupied molecular orbitals (MOs), including the highest (HOMO), are localized on the Cu 3d orbitals (by more than 90%). Below these orbitals, the bonding MOs are formed by the atomic orbitals of the framework O, Al, and Si atoms only.

In all clusters, the Cu^{I} configuration is typically $3d^{10}$ with some population in the 4s and 4p orbitals (0.5−0.6 el.), leading to a Cu net charge of 0.4−0.5. The Cu^{I} bonding to the framework oxygens is thus weak, with no major variation with respect to the number of Al in the ring and the nature of the other counterions. The lowest unoccupied molecular orbital (LUMO) and LUMO + 1 are characteristic of the Na 3s and H 1s, with more Na^+ in the LUMO and more H^+ contributions in the LUMO + 1 for the clusters containing both cations and only Na 3s contributions for the clusters without protons. Depending on the clusters, some small contributions of Cu 4s have been found (≤ 10%). For the clusters with both H^+ and Na^+ cations, the LUMO + 2 is also delocalized on Na 3s and H 1s, whereas this orbital has mainly Cu 4s contributions for the clusters with Na^+ only. In all cases, the LUMO + 3 is dominated by the Cu 4s. In clusters F−H (with Na^+), the LUMO and LUMO + 1 are almost degenerate.

As shown in Table 3, the Cu 3d HOMO values fluctuate little within the A−E and F−H groups but show a clear tendency of destabilization (0.5−0.6 eV) going from H^+/Na^+ to only Na^+ counterions, when one compares the clusters in pairs (A/F, B/G, and C/H).

The ability of zeolite sites to react with molecules has been often characterized by Pearson[36] concepts. The electron-donor and electron-acceptor properties are qualitatively related to HOMO and LUMO energies, that is, in a comparison of two zeolites, the harder base will have a lower-lying HOMO and the higher Lewis acid will have the lowest-lying LUMO.[37,38]

By use of the HOMO energies, one can say that the more protonated solids are globally harder bases than those with more sodium cations, and the solid will thus be more difficult to oxidize. As shown previously, the enhanced catalytic deNO_x activity of Cu−Y for large H^+/Na^+ ratios has to be related to easier local protonation rather than to favored oxidation of the Cu site.[39] The analysis of the LUMO + n behavior is much more difficult since these empty orbitals are delocalized over various cations. It is probable that much larger statistics would be necessary, over several different Al distribution in the clusters (A and F have different general Al content and distributions from the others) and with more examples with mixed counter-

TABLE 3: Bond Order, HOMO and LUMO + *n* Energies, HOMO−LUMO Gaps, and Copper Configuration for Optimized $Cu^{I}Y$ Clusters A−H[a]

	A	B	C	D	E	F	G	H
no. of Al in 6T	1	1	2	2	3	1	1	2
distribution	1	1	1-3	1-4	1-3-5	1	1	1-3
$V(CuO_1)$	0.20	0.17	0.27	0.30	0.28	0.26	0.24	0.30
$V(CuO_3)$	0.28	0.28	0.23	0.29	0.23	0.26	0.26	0.20
$V(CuO_5)$	0.31	0.33	0.28	0.20	0.25	0.30	0.33	0.29
HOMO (eV)	−5.46	−5.29	−5.15	−5.19	−4.83	−4.75	−4.63	−4.60
LUMO (eV)	−2.78	−2.81	−2.70	−2.85	−2.49	−2.36	−2.37	−2.24
LUMO + 1 (eV)	−2.40	−2.50	−2.39	−2.46	−2.19	−2.26	−2.20	−2.23
LUMO + 2 (eV)	−2.24	−2.34	−2.13	−2.11	−1.89	−1.95	−1.88	−1.84
gap (eV)	2.68	2.48	2.45	2.34	2.34	2.39	2.26	2.36
hardness	1.34	1.24	1.23	1.17	1.17	1.20	1.13	1.18
Cu config 3d	9.98	9.97	9.97	9.96	9.96	10.0	10.0	9.96
Cu config 4s	0.33	0.35	0.29	0.29	0.25	0.29	0.29	0.29
Cu config 4p	0.27	0.26	0.28	0.29	0.28	0.27	0.27	0.28

[a] With respect to the distribution pattern of Al in the 6T ring.

ions, to conclude on the variations of the frontier orbitals, and thus on the global properties, like electronegativity or hardness of the solid.

As shown in Table 3, the HOMO−LUMO gap does not change significantly among the various clusters. Even if the HOMO energies increase, the LUMO + *n* energies follow the same trend, keeping their differences almost unchanged.

Even though they are based on a nonextensive sampling of solids, the present results show that the Al and cation distributions and the cocation nature are not decisive factors in determining the global electronic properties of the zeolites.

III.6. Molecular Electrostatic Potential Energy. The electrostatic interaction energy (MEP) between the molecular electronic and nuclear charge distribution and an external point charge is often used to approximate the position of a counterion in an anionic species. In zeolites, negative MEP wells are found in the vicinity of the framework oxygens, with the lowest ones associated with the oxygens of AlO_4 tetrahedra. In this study, all cations are monocharged and thus compensate the negative charge of one framework Al. Whereas +2 or +3 cations compensating two or three Al may be positioned quite far from the related AlO_4 tetrahedra, +1 cations are generally located in their close vicinity.

MEP values have been evaluated for the anions corresponding to clusters A−H, after removal of the Cu^{I} cation, keeping the optimized geometry of the neutral systems. These calculations are thus fast and, by comparison with the full DFT results, can shed some light on the major electronic effects that govern the Cu−framework bonding. MEP values have also been calculated for cluster C, optimizing the anion structure ("optimized"), thus providing an estimate of the structural rearrangement from the anion to the neutral Cu^{I} system.

Figure 6, which presents the MEP contours for one Al, model B (panel a), and two Al, model C (panel b), with the geometries of the neutral systems ("nonoptimized"), is very representative of the MEPs obtained for all clusters.

A MEP contour, higher than the deepest minimum by approximately 0.4−0.6 eV, forms a central basin with three lobes, at a distance of 1.35−165 Å from the O_1, O_3, and O_5 oxygens. These oxygens are pointing toward the center of the 6T ring and correspond, in general, to smaller (AlOSi) angles than the three other ones, which are pointing outward the ring. There is indeed a correlation between smaller angles and deeper MEPs.[40] The analysis of these basins for the optimized and nonoptimized anions of model C shows the presence of comparable MEP basins, despite the fact that similar contours are obtained for lower potential values (Figures 6b and 7). Indeed, the MEP minima after optimization are less negative by about 1.7 eV, due to a spatial redistribution of the density. This effect is connected with the relaxation of the structure, affecting essentially the positions of the inward O_1, O_3, and O_5 oxygens, which differ by about 0.2 Å with respect to the nonoptimized structure (Figure 7). Nevertheless, the conclusions derived from the nonoptimized anions remain valid in the case of optimized anions.

The electrostatic potential energy minima have very similar values when models A−E, 5.7 ± 0.2 eV, and F−H, 6.35 ± 0.1 eV, are compared. For all clusters, no other minima could be found above or below the 6T ring.

From these results, several conclusions can be drawn: (i) the shape of the MEP basins is determined by the structure of the 6T ring itself, that is, by the three inward and three outward oxygens; (ii) the presence of more pronounced MEP wells in the 6T ring is linked to the number of Al in the ring and their depths correlate with the AlOSi angles; (iii) the depths of the MEP wells show a small but clear dependency on the nature of the compensating cations (H^+ versus Na^+); the electrostatic framework cation interaction within the 6T ring is slightly larger when the cocations are Na^+; (iv) all the minima are located in the plane formed by O_1, O_3, and O_5.

Upon comparing these conclusions with those drawn from full DFT calculations, we can state that electrostatic interactions are the major factors governing site II geometry and the Cu^{I}−zeolite bonding. The same result was also obtained from contour maps of the electron localization function (ELF) of Becke and Edgecombe.[41,42] Indeed, we have shown, in section III.5, that whatever the Al distribution in the 6T ring, Cu^{I} is bonded to the O_1, O_3, and O_5 oxygens with two short bonds and one slightly longer, that is, with a coordination close to 3, and that their valence bond orders, typical of weak bonds, are all very comparable.

Finally, another important conclusion is that, in all clusters, the MEP minima connected with the 6T ring are all located in the O_1, O_3, O_5 plane, independently of the number of Al and of the nature of the other counterions. This is illustrated in Figure 6 by the absence of any other negative MEP well below or above this plane. Therefore, the existence of two positions for Cu, one inside the 6T ring and one shifted by about 1 Å into the supercage, cannot be explained either by the nature of the counterions or by the distribution of Al in the 6T ring.

IV. Conclusion

In this work, we have studied the local structure of a Cu^{I} site II in a CuY zeolite and its relationships with the framework Al

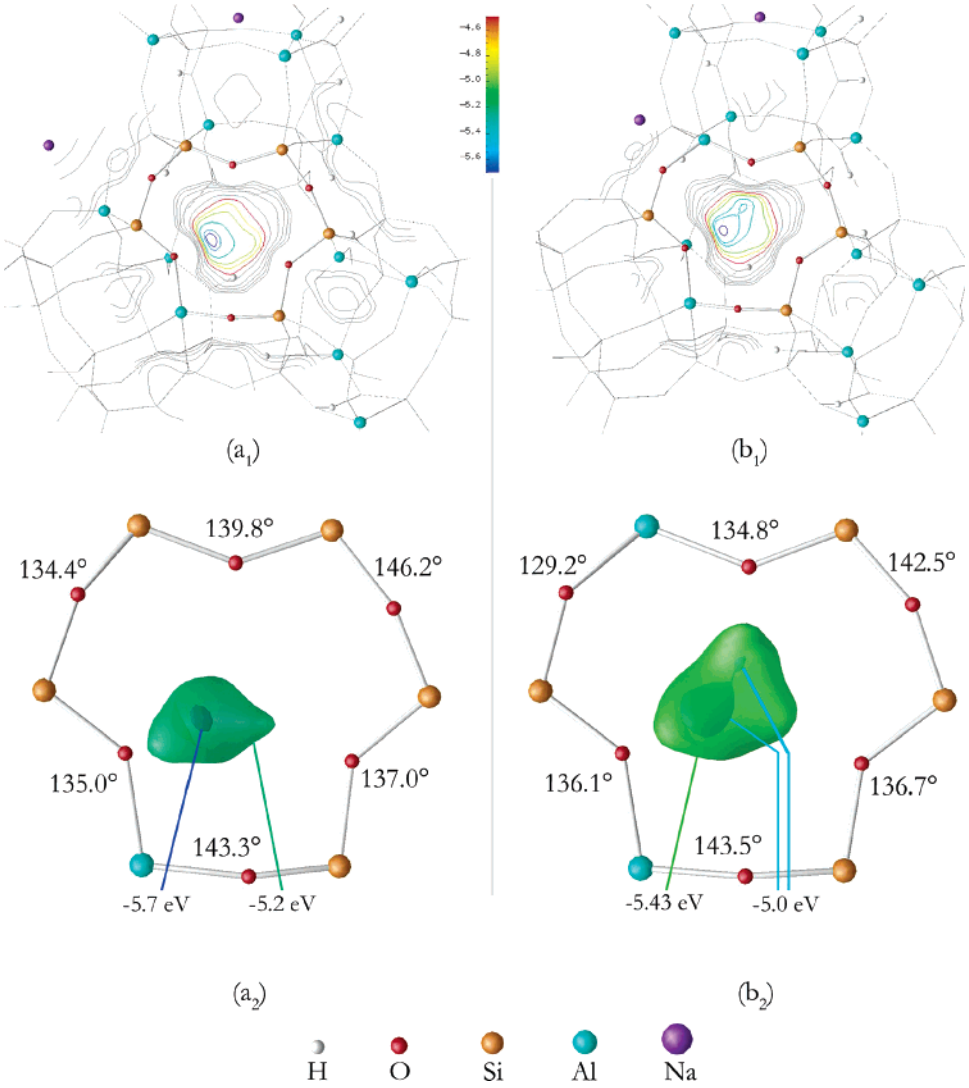

Figure 6. (a_1, b_1) Molecular electrostatic potential maps drawn within the O_1, O_3, O_5 plane, and (a_2, b_2) 3D MEP isovalues associated with the calculated 6T ring bond angles. Structures a_1 and a_2 are related to the anionic cluster of model B obtained after removal of the Cu^{I}; structures b_1 and b_2 are related to the anionic cluster of model C obtained after removal of the Cu^{I}.

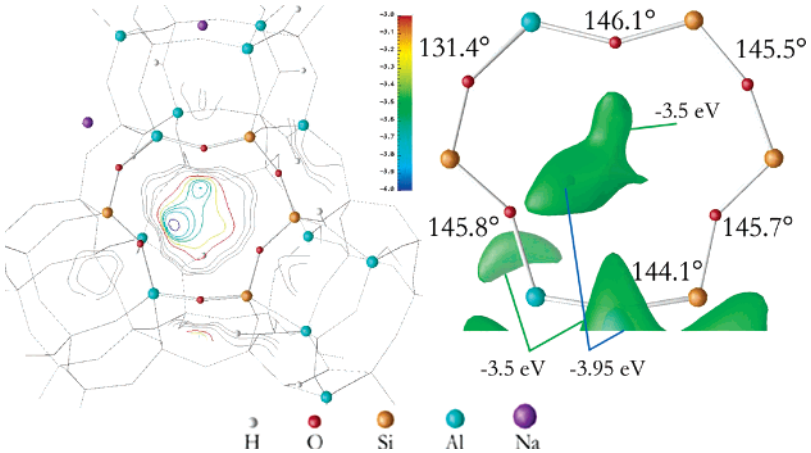

Figure 7. (Left) Molecular electrostatic potential maps of the optimized anionic cluster model C drawn within the O_1, O_3, O_5 plane. (Right) 3D MEP isovalues associated with the calculated 6T ring bond angles.

distribution and with the nature of the cocations. For this purpose, we have compared the structures of models with different Al contents and distribution patterns and two sets of extraframework cations (H^+/Na^+ and Na^+).

In all models, Cu^{I} has been found located within the plane defined by the three oxygens pointing inside the 6T ring of site II. The Cu^{I} position varies slightly within this plane, depending on the presence and distribution of Al inside the 6T ring, but these variations are not substantial enough to define different types of site II, as has been proposed from diffraction experiments. All the models, after geometry optimization, contain a copper coordinated to three framework oxygens, with one bond

of about 2.26 Å and two shorter bonds of about 2.07 Å, indicating that the local deformations of the 6T ring break the ideal C_3 symmetry.

In contrast, the large experimental temperature factors found for this site by experimental methods lead to uncertainties of about 0.150 Å (XRD) and 0.224 Å (HRND) for the Cu−O bonds, revealing the difficulty to reach an accurate local description by use of the overall high symmetry of the fully siliceous solid.

Hence, comparing calculated and experimental results allows us to propose that (i) there is only one site II occupied by Cu (assertion confirmed by the MEPs analysis); (ii) the two different Cu−O bonds values found experimentally at 2.03 and 2.21 Å by XRD are related to the local symmetry breaking due to the presence of Al in the 6T ring; and (iii) this pattern (two short and one longer Cu−O bonds) remains independent of the Al topology and cocation nature.

The geometry and electrostatic properties at site II, as well as the frontier orbital nature and relative energies, do not show a clear dependency on the Al and cation distribution (with a slight effect of the cocation nature), in accordance with the common experimental experience, that is, similar properties for solids within a range of 2.5−5 Si/Al ratios. Taking also into account the experimental increased deNO_x activity of CuY with large H^+/Na^+ ratios leads us to propose that specific catalytic behaviors must be correlated with local response properties, such as the local acid strength (easier deprotonation for specific locations) or, in other reactions, specific local architecture or confinement.

References and Notes

(1) Guth, J. L.; Caullet, P.; Seive, A.; Patarin, J.; Delprato, F. In *Guidelines for Mastering the Properties of Molecular Sieves*; Barthomeuf, D., Derouane, E. G., Hölderich, W., Eds.; Plenum: New York, 1990; p 69.

(2) Klinowski, J.; Ramdas, S.; Thomas, J. M.; Fyfe, C. A.; Hartman, J. S. *J. Chem. Soc.* **1982**, *78*, 1025.

(3) Plévert, J.; Di Renzo, F.; Fajula, F.; Chiari, G. *J. Phys. Chem. B* **1997**, *101*, 10340.

(4) Nusterer, E.; Blöchl, P. E.; Schwarz, K. *Angew. Chem., Int. Ed. Engl.* **1996**, *35*, 175.

(5) Jeanvoine, Y.; Angyan, J. G.; Kresse, G.; Hafner, J. *J. Phys. Chem. B* **1998**, *102*, 5573.

(6) Campana, L.; Selloni, A.; Weber, J.; Goursot, A. *J. Phys. Chem.* **1997**, *101*, 9932.

(7) Kessi, A.; Delley, B. *Int. J. Quantum Chem.* **1998**, *68*, 135.

(8) Profeta, M.; Mauri, F.; Pickard, C. J. *J. Am. Chem. Soc.* **2003**, *125*, 541.

(9) Termath, V.; Haase, F.; Sauer, J.; Hutter, J.; Parrinello, M. *J. Am. Chem. Soc.* **1998**, *120*, 8512.

(10) Stich, I.; Gale, J. D.; Terakura, K.; Payne, M. C. *Chem. Phys. Lett.* **1998**, *283*, 402.

(11) Demuth, T.; Hafner, J.; Benco, L.; Toulhouat, H. *J. Phys. Chem. B* **2000**, *104*, 4593.

(12) White, J. C.; Hess, A. C. *J. Phys. Chem.* **1993**, *97*, 8703.

(13) Rozanska, X.; van Santen, R. A.; Demuth, T.; Hutschka, F.; Hafner, J. *J. Phys. Chem. B* **2003**, *107*, 1309.

(14) Rozanska, X.; Barbosa, L. A. M. M.; van Santen, R. A. *J. Phys. Chem. B* **2005**, *109*, 2203.

(15) Rozanska, X.; Garcia-Sanchez, M.; Hensen, J. M.; van Santen, R. A. *C. R. Chim.* **2005**, *8*, 509.

(16) Bucko, T.; Hafner, J.; Benco, L. *J. Phys. Chem. A* **2004**, *108*, 11388.

(17) Elanany, M.; Koyama, M.; Kubo, M.; Broclawik, E.; Miyamoto, A. *Appl. Surf. Sci.* **2005**, *246*, 96.

(18) Shetty, S.; Kanhere, P. D.; Goursot, A.; Pal, S. *Chem.—Eur. J.* **2006**, *12*, 518.

(19) Milas, I.; Nascimento, M. A. C. *Chem. Phys. Lett.* **2000**, *418*, 364.

(20) Rungsirisakun, R.; Jansang, B.; Pantu, P.; Limtrakul, J. *J. Mol. Struct.* **2005**, *733*, 239.

(21) Löwenstein, W. *Am. Mineral.* **1942**, *39*, 92.

(22) Gallezot, P.; Ben Taarit, Y.; Imelik, B. *J. Catal.* **1972**, *26*, 295.

(23) Smith, J. V. *Adv. Chem. Ser.* **1971**, *101*, 171.

(24) Maxwell, I. E.; de Boer, J. J. *J. Phys. Chem.* **1975**, *79*, 1874.

(25) Palomino, G. T.; Bordiga, S.; Zecchina, A.; Marra, G. L.; Lamberti, C. *J. Phys. Chem.* **2000**, *104*, 8641.

(26) Fowkes, A. J.; Ibberson, R. M.; Rosseinsky, M. J. *Chem. Mater.* **2002**, *14*, 590.

(27) Bordiga, S.; Garonne, S.; Lamberti, C.; Zecchina, A.; Areán, C. O.; Kazansky, V. B.; Kustov, L. M. *J. Chem. Soc.* **1994**, *90*, 3367.

(28) Bordiga, S.; Scarano, D.; Spoto, G.; Zecchina, A.; Lamberti, C.; Areán, C. O. *Vib. Spectrosc.* **1993**, *5*, 69.

(29) Cerius2 Molecular modeling software for materials research; Accelrys; Biosym Technologies: San Diego, CA, 1993.

(30) Koester, A. M.; Calaminici, P.; Flores, R.; Geudtner, G.; Goursot, A.; Heine, T.; Janetzko, F.; Patchkovskii, S.; Reveles, J. U.; Vela, A.; Salahub, D. R. deMon 2K, 2004.

(31) Reveles, J. U.; Koester, A. M. *J. Comput. Chem.* **2004**, *25*, 1109.

(32) Perdew, J. P.; Burke, K.; Ernzerhof, M. *Phys. Rev. Lett.* **1996**, *77*, 3865.

(33) Godbout, N.; Salahub, D. R.; Andzelm, J.; Wimmer, E. *Can. J. Phys.* **1992**, *70*, 560.

(34) Spoto, G.; Zecchina, A.; Bordiga, S.; Ricchiardi, G.; Matra, G.; Leofanti, G.; Petrini, G. *Appl. Catal. B* **1994**, *3*, 151.

(35) It is generally admitted that the average bond-length error from GGA calculations is in the range 0.03−0.06 Å, depending on the system; the metal−ligand bond lengths may be overestimated by the largest error (0.06 Å).

(36) Pearson, R. G. *J. Am. Chem. Soc.* **1963**, *85*, 3533.

(37) Corma, A.; Zicovich-Wilson, C.; Viruela, J. *Phys. Org. Chem.* **1994**, *7*, 364.

(38) Sastre, S.; Corma, A. *Chem. Phys. Lett.* **1999**, *302*, 447.

(39) Delahay, G.; Villagomez, E. A.; Ducere, J.-M.; Berthomieu, D.; Goursot, A.; Coq, B. *ChemPhysChem* **2002**, *3*, 686.

(40) Goursot, A.; Fajula, F.; Daul, C.; Weber, J. *J. Phys. Chem.* **1988**, *92*, 4456.

(41) Becke, A. D.; Edgecombe, K. E. *J. Chem. Phys.* **1990**, *92*.

(42) Silivi, B.; Savin, A. *Nature (London)* **1994**, *371*, 683.